NIH Public Access
Author Manuscript
J Solgel Sci Technol. Author manuscript; available in PMC 2013 July 05.

Published in final edited form as:
J Solgel Sci Technol. 2010 February ; 53(2): 459–465. doi:10.1007/s10971-009-2114-z.

Aminosilane as an effective binder for hydroxyapatite-gelatin nanocomposites

Tzy-Jiun M. Luo[1], **Ching-Chang Ko**[2], **Chi-Kai Chiu**[1], **Jacob Llyod**[1], and **Uk Huh**[1]

[1]Department of Materials Science and Engineering, North Carolina State University, Raleigh, NC 27695, USA Mark_Luo@ncsu.edu

[2]Department of Orthodontics, University of North Carolina, Chapel Hill, NC 27599-7450, USA koc@dentistry.unc.edu

Abstract

Aminosilane has been explored as an alternative chemical linker to facilitate the binding and solidification of hydroxyapatite-gelatin nanocomposite at room temperature, which was synthesized using co-precipitation method in the presence of gelatin. This aminosilane treatment was found effective at low concentration (~25 μL/mL) and the solidification and dehydration of hydroxyapatite-gelatin slurry completes within hours depending on the amount of aminosilane. The resulting sample exhibits compressive strength of 133 MPa, about 40% higher than glutaraldehyde treated samples, and shows good biocompatibility based on cell adhesion, proliferation, alkaline phosphate synthesis, and mineralization studies.

Keywords

Aminosilane Hydroxyapatite; Nanocomposite; Osteoblast; Biomaterials

1. Introduction

Ceramic biomaterials based on biomimetic approaches have attracted much attention because they are functionally and structurally compatible with the calcified tissue [1–3]. An example is the engineering of natural bone substituent that contains hydroxyapatite and collagen [4, 5]. nanocrystalline hydroxyapatite has been successfully synthesized at a feasible quantity, making it possible for immediate biomedical uses [6]. However, conversion of crystalline hydroxyapatite from solution state to solid form usually requires multiple steps including purification, concentration, cross-linking, and solidification. To cope with this process, cross-linking reagents such as glutaraldehyde [7], polyvinyl alcohol [8], carbondiimide and succinimide [9], have been widely employed. Alternative approach utilizes polymer matrix to encapsulates mineral components and form a connected structure [10, 11]. In general, surface treatment on the mineral components is often needed in order to achieve reasonable mechanical strength. In search for a more biocompatible synthetic approach, we utilized a unique aminosilica precursor, bis[3-(trimethoxysilyl)propyl]ethylenediamine (enTMOS) [12, 13], which serves as both matrix and binder for hydroxyapatite nanocrystals, and explore it as a rapid approach for bioceramics fabrication. Similar sol–gel process has been studied for its biocompatibility as reported by the literature [14, 15]. While aminosilane has also been reported by Dupraz et al. [16] to bind to hydroxyapatite, here sol–gel process was utilized to synthesize aminosilica matrix that involves aminosilane chemical and hydroxy-apatite-gelatin (HAP-Gel) without changing the pH of the solution. Gelation of aminosilane was induced by hydroxyapatite and gelatin in the solution and its dehydration spontaneously occurred afterwards and completed within 24 h (Fig. 1a). In this paper, we present synthesis, characterization and cell culture

NIH-PA Author Manuscript
NIH-PA Author Manuscript
NIH-PA Author Manuscript

NIH-PA Author Manuscript

NIH-PA Author Manuscript

NIH-PA Author Manuscript

studies of this new material (GEMOSIL). The results show that it exhibits cytocompatibility, improved mechanical strength, and unique nanostructures. Similar procedure if performed using tetramthylorthosilicate (TMOS) or tetraethylorthosilicate (TEOS) often lead to reduced cellular activities. Furthermore, it was also found that the unique molecular structures of aminosilane and the interactions between aminosilica and hydrxyapatite-gelatin complexes contribute to its rapid solidification and dehydration process.

2. Experimental procedure

2.1 Preparation of hydroxyapatite-gelatin slurry

The stock solution of hydroxapaptite-gelatin (HAP-Gel) was prepared according to the reported co-precipitation method [6]. In general, a 1.4 L of solution containing 0.275 M $Ca(OH)_2$ was mixed with a 1.2 L of 60 mM H_3PO_4 solution. Then, 5.0 g of gelatin (MW = 50–250 kD) in DI water was slowly added to the mixture using a peristaltic pump, and the mixture was maintained at 38 °C and pH 8.0 for 24 h. The resulting HAP-Gel slurry was centrifuged at 70,000 × g for 5 min. After removing the supernatant, the residue was suspended in equal volume of methanol and used as a HAP-Gel stock solution.

2.2 Synthesis of hydroxapatite-gelatin-aminosilica thin films

The synthetic method described here can be scaled up depending on the quantity of composite material that was needed. Aminosilane was added to the HAP-Gel stock solution at a volume ratio of 25 μL enTMOS for every 1 mL of HAP-Gel stock solution, then the mixture was immediately sonicated at room temperature for 5 min. This step resulted in a semi-transparent solution that does not solidify for several hours. To coat the films on petri dish or multi-well culture dish, the mixture was dropped onto each well at a volume to area ratio of 12.5 $\mu L/cm^2$. The coating was allowed to dry for 4 h and then age for another 24 h before use. Once dried, the film on petri dish exhibited hydrophobic property and did not delaminate even in the culture medium.

2.3 Synthesis of hydroxyapatite-gelatin-aminosilica bulk samples

HAP-Gel stock solution was mixed with enTMOS at a volume ratio of 25 μL for every 1 mL of HAP-Gel stock solution. The solution was mixed vigorously and then sonicated for 5 min followed by 5 min of centrifugation at 70,000 × g. After removing the supernatant, the residue was compressed against a 0.45 μm syringe filter to remove excessive liquid. The remaining concentrated slurry was transferred to a cylinder shape container and allowed to dry at room temperature.

2.4 Transmission electron microscopy

HAP-Gel stock solutions with and without enTMOS were dropped onto a gold TEM grid (Electron Microscopy Sciences Inc.) followed by drying in the air. Images were taken on Philips CM12 (FEI Co.) transmission electron microscope using an accelerated voltage of 80 KV.

2.5 Atomic force microscope

AFM images were taken on a Caliber atomic force microscope (Veeco Inc.) using silicon nanoprobe cantilevers as scanning probes. The acoustic tapping mode was used on all measurements. The tapping amplitude of cantilever was adjusted to 4.5 V prior to sample engagement. Images were measured with a voltage set point of 2.8 V and a scan rate of 0.5–1 Hz. To avoid image distortion, scanning were carried out with active closed-loop on all X, Y, and Z axes. In general, four image modes were obtained from each measurement that includes tapping amplitude, phase, deflection and height modes.

NIH-PA Author Manuscript

NIH-PA Author Manuscript

NIH-PA Author Manuscript

2.6 Powder X-ray diffraction (XRD)

GEMOSIL samples after synthesized, dried in the air, and grinded into powder were placed in the sample holder of a Philips X-ray automated powder diffractometer equipped with a Cu target and a Ge postsample monochromater. To obtain the X-ray diffraction pattern of a pure enTMOS gel, enTMOS was solidified by adding minimum of water, dried, and grinded into powder before placing on the XRD.

2.7 Compression test

Five cylindrical rods (2 mm in diameter and 4 mm in height) were made from GEMOSIL. Each sample was compressed using an Instron 4204 (Canton, MA, USA) at the speed of 0.5 mm/min. Stress–strain curve was recorded. Averaged ultimate compressive strength was reported using the highest stress value of each sample.

2.8 Cell culture study

Osteoblasts, MC3T3-E1, were cultured in 96-well plates (Falcon, Becton, Dickinson Labware, Frankin Lakes, NJ, USA), where all wells were coated with GEMOSIL. Cells were seeded at a density of 1 9 10^4 per milliliter using αMEM medium supplemented with 10% of FBS and 1% penicillin/streptomycin under 37 °C, 5% CO2 atmosphere. Live and death assay (LIVE/DEADViability/Cytotoxicity Kit L-3224, Invitrogen, Carlsbad, CA, USA) was conducted to provide visualization of cell viability 4 days after cultivation. Cell proliferation was measured at 1, 4, 7, and 10 days after seeding. At the end of the designed cultivation period, 20 μL of CellTiter reagent (CellTiter 96®Aqueous One Solution Proliferation Assay, Promega Co, Madison, WI, USA) was added to each well and the plate was incubated at 37 °C for 1 h according to manufacture's instruction. The quantity of formazan product was determined based on UV–VIS absorbance at 490 nm, since its quantity directly proportional to the number of living cells in culture. The control sample was carried out on 96-well plates without GEMOSIL coating. In general, five samples were tested at each time point for each group (n = 5).

A pilot assessment for cell differentiation on the material was performed using the assay for alkaline phosphatase (ALP) protein activity and alizarin red for mineralization stain. The 35 mm Petri dishes coated with GEMOSIL were used for differentiation studies. Sixteen coated dishes for ALP activity were equally divided into four groups (day 0, 3, 7 and 10 after cells reached confluence.) Another sixteen non-coated dishes were used for the control to compare ALP activity with the corresponding groups. Two additional coated dishes were used to assess mineralization; the cells in these two dishes were kept up to 21 days after cell confluence. Visual indication for calcification was achieved using Alizarin Red staining package (Acros Organics, Geel, Belgium) following manufacturer's protocol.

For ALP activity and mineralization, cells were maintained in αMEM medium containing 10% FBS, plated onto 35 mm dishes at a density of 1×10^5 cells/mL, cultured for 3 days (reaching confluence) and the same growth medium was supplemented with 10 mM B-glycerophos-phate and 0.2 mM ascorbic acid. For ALP activity assay, cell lysates were collected and ALP activity was measured using Alkaline Phosphatase Yellow (pNPP; p-nitrophe-nylphosphate) Liquid Substrate System for ELISA (Sigma, St. Louis, MO, USA) as reported by Parisuthiman [17]. The protein concentration was measured by DC protein assay kit (Bio-Rad) and ALP activity was calculated as mL of pNP/min/total protein. The assay was also performed in triplicate to confirm reproducibility.

NIH-PA Author Manuscript

NIH-PA Author Manuscript

NIH-PA Author Manuscript

3 Results and discussion

Depending on the concentration of aminosilane, the appearance of GEMOSIL was semi-transparent to opaque and the drying time varied from hours to days. In general, more enTMOS remains in the sample, more transparent sample with a shorter drying time was obtained. When prepared directly from HAP-Gel stock solution without the chemical binders, samples were semi-transparent whitish at dry, and no shrinkage was observed (Fig. 1b, HAP-Gel). On the contrary, samples containing aminosilane showed an average of 30% shrinkage (Fig. 1b, GEMOSIL). The accurate shrinkage was estimated based on reduction on the diameter of GEMOSIL cylindrical rods after created from the round shape culture well of culture plate (0.8 cm in diameter). In general, shrinking is caused by the collapsing of the porous structures of matrix when solvent is evaporated, as reported by many investigators [18–20]. Shrinking was observed on most of the samples except for thin-film samples, and therefore thin films were used to examine their biocompatibility and surface properties while bulk samples were used to determine their mechanical strength. The minimum ratio of aminosilane to HAP-Gel stock solution was determined to be no less than 25 μL/mL in order to maintain both silica and HAP-Gel at reasonable quantity. Without adding HAP-Gel component, a methanol solution containing 25 μL/mL aminosilane will not result in solid sample even when dry. We also observed that HAP-Gel within enTMOS matrix caused faster dehydration rate as compared to a pure enTMOS gel. It was found that within 5 min of gelation, solvent was quickly secreted from the sample, which is possibly caused by shrinking of enTMOS matrix itself. We postulated the packing arrangement of hydroxyapatite nanocrystals should be affected by aminosilane, and therefore the arrangement of GEMOSIL nanocrystals was examined using transmission electron microscopy (TEM). Figure 2a clearly shows those needle shape hydroxyapatite crystals have a length of 200 nm and a width of 5–10 nm in the aggregate. Some hydroxyapatite nanocrystals in the form of rectangular shape are also observed in the slurry. Since gelatin acts as the template and induces nucleation of hydroxyapatite, the long axis of hydroxyapatite is parallel to the longitudinal direction of the gelatin structure (Fig. 2b). While in GEMOSIL, aminosilica exists as a solid matrix surrounding hydroxyapatite nanocrystals, which results in a higher density of HAP-GEL nanocrystals (Fig. 2c). Several localized high-density aggregation of nanocrystals were observed on the TEM micrograph and the needle shape HAP-Gel crystals have been well preserved in the silica matrix. Due to the presence of amorphous aminosilica matrix, the crystalline hydroxyapatite nanocrystals are not clearly visible (Fig. 2d).

X-Ray diffraction patterns of GEMOSIL show that three distinct peaks associated with hydroxyapatite diffraction patterns are overlapping with two broad diffraction bands (Fig. 3a). X-Ray diffraction peaks of hydroxyapatite as shown in Fig. 3b are 26°, 32°, 40°, and 47°, which correspond to peaks (002), (211), (310), and (222), respectively. Compared to the diffraction pattern of HAP-Gel nanocrystals, the broader peak at 20°is associated with the spacing between silicon atoms of the amorphous amino-silica solid [21]. XRD results show that the crystal structures of hydroxyapatite were maintained within the aminosilica matrix, which is also supported by the TEM results. Both indicate aminosilane hydrolyze and polymerize surrounding HAP crystals and encapsulate HAP crystals.

The IR absorption spectrum for HAP-Gel exhibits several characteristic peaks (Fig. 4a), and they are amide absorption at 1,647 cm^{-1}, –CH2– bending at 1,455 cm^{-1}, and PO_4 band at 1,302 cm^{-1}. Figure 4b is the IR spectrum of a pure aminosilica solid, which was synthesized from enTMOS. Characteristic peaks include C–H stretching at 2,937 cm^{-1}, N–H bending at 1,653 cm^{-1}, –CH2– bending at 1,473 cm^{-1} . Si–O–Si stretching is 1,029 and 1,118 cm^{-1}, indicating the formation of aminosilica matrix. Figure 4c is the IR spectrum of GEMOSIL and it shows that the spectrum is dominated by enTMOS. Three functional groups on

NIH-PA Author Manuscript

NIH-PA Author Manuscript

NIH-PA Author Manuscript

enTMOS with distinct interactions with HAP-Gel are N–H bending (1,641 cm $^{-1}$), –CH2– bending (1,468 cm^{-1}), and Si–O–Si stretching (1,126.8 cm $^{-1}$). Red shift of N–H bending indicates the presence of hydrogen bonding with HAP-Gel, and blue shift of Si–O–Si absorption indicates possible interactions of SiO2 and $PO4^{3-}$of hydroxyapatite. This interaction also explains why silane chemicals have been utilized to improve the bonding between hydroxyapatite and polymer matrix as reported by the literature [22, 23]. A broader 3,500 cm $^{-1}$ (O–H) indicates massive hydrogen bonding interactions that result from the presence of HAP-Gel crystals. FT-IR results confirm that both amino and silanol functional groups of enTMOS contribute to the binding of HAP-Gel. We conclude that such interactions between aminosilica and hydrxyapatite regions contribute to its rapid solidification and dehydration process.

GEMOSIL film was also examined using AFM, which shows that the surface topography is dominated by the nanostructures of hydroxyapatite nanocrystals. The surface roughness (Ra) of GEMOSIL is 70 nm with an average grain size at 730 nm (Fig. 5a). This feature size is significantly bigger than the needle shape hydroxyapatite crystals observed on the TEM. It indicates the formation of larger aggregates is possibly induced by aminosilane. The pure HAP-Gel film has smaller aggregates (grain size~500 nm) and its roughness (Ra) is 35 nm (Fig. 5b). Two AFM images show the effects of aminosilane, which serves as binders and space fillers. As for pure aminosilica sample, its surface exhibit much smoother topography and without surface granulized features (data not shown). To determine its mechanical strength, the resulting compressive strength for GEMOSIL nanocomposites was 133 ± 39 MPa, which is about 40% higher than the HAP-GEL that was cross-linked by glutaraldehyde [24].

Cell culture studies were carried out on the surface of GEMOSIL using osteoblast cells (MC3T3-E1) and the results found that osteoblast cells adhered and grew normally on the surfaces of the GEMOSIL matrix. The ratio between the live cells versus dead cells were similar on both GEMOSIL coated dish and the control (Fig. 6). The cell growth curves are no difference between the coated dish and the control too (Fig. 7). Results also showed that there were no differences in alkaline phosphatase activity (synthesis function) between cells grown on the material and the control (Fig. 8a). Alizarin red stain further confirmed the ability of cell mineralization on the GEMOSIL surface (Fig. 8b). Because of the positive cellular responses for both proliferation and differentiation experiments, our preliminary data suggest that GEMOSIL can be a candidate for bone replacement. The results show that it exhibited cytocompatibility, improved mechanical strength, and unique nanostructures.

Conclusion

Hydroxyapatite-gelatin has been successfully solidified from room temperature and solution process using enTMOS as a chemical linker to produce thin film and bulk samples. Morphology of nanocrystals and crystalline structures of hydroxyapatite have been preserved after solidification process. In addition, enTMOS treatment increases compressive strength by 40% compared to glutaraldehyde linker, and the resulting GEMOSIL exhibits good osteoblast cell compatibility.

Acknowledgments

This work is supported, in part, by, NC Biotech Center Grant#2008-MRG-1108. CCK also thanks NIDCR K08DE018695 and American Association of Orthodontists Foundation for their financial support.

NIH-PA Author Manuscript

NIH-PA Author Manuscript

NIH-PA Author Manuscript

References

1. Green D, Walsh D, Mann S, Oreffo ROC. The potential of biomimesis in bone tissue engineering: lessons from the design and synthesis of invertebrate skeletons. Bone. 2002; 30:810–815. [PubMed: 12052446]
2. Boskey AL. Will biomimetics provide new answers for old problems of calcified tissues? Calcif Tissue Int. 1998; 63:179–182. [PubMed: 9701619]
3. Murugan R, Ramakrishna S. Development of nanocomposites for bone grafting. Compos Sci Technol. 2005; 65:2385–2406.
4. Wahl DA, Czernuszka JT. Collagen-hydroxyapatite composites for hard tissue repair. Eur Cell Mater. 2006; 11:43–56. [PubMed: 16568401]
5. Wu TJ, Huang HH, Lan CW, Lin CH, Hsu FY, Wang YJ. Studies on the microspheres comprised of reconstituted collagen and hydroxyapatite. Biomaterials. 2004; 25:651–658. [PubMed: 14607503]
6. Chang MC, Ko CC, Douglas WH. Preparation of hydroxyapatite-gelatin nanocomposite. Biomaterials. 2003; 24:2853. [PubMed: 12742723]
7. Chang MC, Ko CC, Douglas WH. Conformational change of hydroxyapatite/gelatin nanocomposite by glutaraldehyde. Biomaterials. 2003; 24:3087–3094. [PubMed: 12895581]
8. Chang MC, Ko CC, Douglas WH. Modification of hydroxyapatite/gelatin composite by polyvinylalcohol. J Mater Sci. 2005; 40:2723–2727.
9. Chang MC, Douglas WH. Cross-linkage of hydroxyapa-tite/gelatin nanocomposite using imide-based zero-length cross-linker. J Mater Sci Mater Med. 2007; 18:2045–2051. [PubMed: 17558474]
10. Higashi S, Yamamuro T, Nakamura T, Ikada Y, Hyon SH, Jamshidi K. Polymer hydroxyapatite composites for biodegradable bone fillers. Biomaterials. 1986; 7:183–187. [PubMed: 3013326]
11. Yunos DM, Bretcanu O, Boccaccini AR. Polymer-bioceramic composites for tissue engineering scaffolds. J Mater Sci. 2008; 43:4433–4442.
12. Ko, CC.; Luo, TJM.; Ma, A. Hydroxyapatite/GEMOSIL nanocompsoite. In: Narayan, R.; Colombo, P., editors. Advances in bioceramics and porous ceramics: ceramic engineering and science proceedings. Wiley; New York: 2008.
13. Rao MS, Dubenko IS, Roy S, Ali N, Dave BC. Matrix-assisted biomimetic assembly of ferritin core analogues in organosilica sol-gels. J Am Chem Soc. 2001; 123:1511–1512. [PubMed: 11456731]
14. Anderson SI, Downes S, Perry CC, Caballero AM. Evaluation of the osteoblast response to a silica gel in vitro. J Mater Sci Mater Med. 1998; 9:731–735. [PubMed: 15348931]
15. Carturan G, Dal Toso R, Boninsegna S, Dal Monte R. Encapsulation of functional cells by sol–gel silica: actual progress and perspectives for cell therapy. J Mater Chem. 2004; 14:2087–2098.
16. Dupraz AMP, de Wijn JR, vanderMeer SAT, de Groot K. Characterization of silane-treated hydroxyapatite powders for use as filler in biodegradable composites. J Biomed Mater Res. 1996; 30:231–238. [PubMed: 9019488]
17. Parisuthiman D, Mochida Y, Duarte WR, Yamauchi M. Biglycan modulates osteoblast differentiation and matrix mineralization. J Bone Miner Res. 2005; 20:1878–1886. [PubMed: 16160746]
18. Brinker, CJ.; Scherer, GW. Sol-gel science. Academic Press; San Diego: 1990.
19. Hench LL, West JK. The sol-gel process. Chem Rev. 1990; 90:33–72.
20. Helbig JM, Hutter M, Schonholzer UP. Lack of syneresis during gelation of dense colloidal suspensions. J Colloid Interf Sci. 2000; 222:46–50.
21. Lana SLB, Seddon AB. X-ray diffraction studies of sol–gel derived ORMOSILs based on combinations of tetramethoxysilane and trimethoxysilane. J Sol-Gel Sci Technol. 1998; 13:461–466.
22. Sousa RA, Reis RL, Cunha AM, Bevis MJ. Coupling of HDPE/hydroxyapatite composites by silane-based methodologies. J Mater Sci Mater Med. 2003; 14:475–487. [PubMed: 15348431]
23. Wang M, Bonfield W. Chemically coupled hydro-xyapatite-polyethylene composites: structure and properties. Biomaterials. 2001; 22:1311–1320. [PubMed: 11336303]

24. Ko CC, Oyen M, FA M, Hu W-S. Mechanical properties and cytochompatibility of biomimetic hydroxyapatite-gelatin nanocomposites. J Mater Res. 2006; 21:3090–3098.

NIH-PA Author Manuscript

NIH-PA Author Manuscript

NIH-PA Author Manuscript

NIH-PA Author Manuscript

NIH-PA Author Manuscript

NIH-PA Author Manuscript

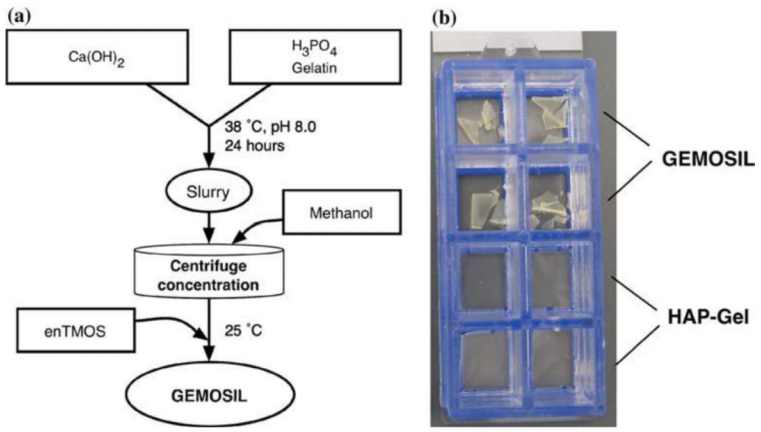

Fig. 1.

a Flow chart of stepwise procedure for producing enTMOS bound hydroxyapatite-gelatin nanocomposites (GEMOSIL). After slurry was synthesized, hydroxyapatite was re-suspended in a methanol solution. GEMOSIL was obtained after mixing with enTMOS followed by sonication, gelation, and dehydration. **b** Effects of aminosilane (enTMOS) on the solidification process of HAP-Gel. Strong binding between enTMOS and HAP-Gel resulted in sample cracking after shrinking occurs.

NIH-PA Author Manuscript

NIH-PA Author Manuscript

NIH-PA Author Manuscript

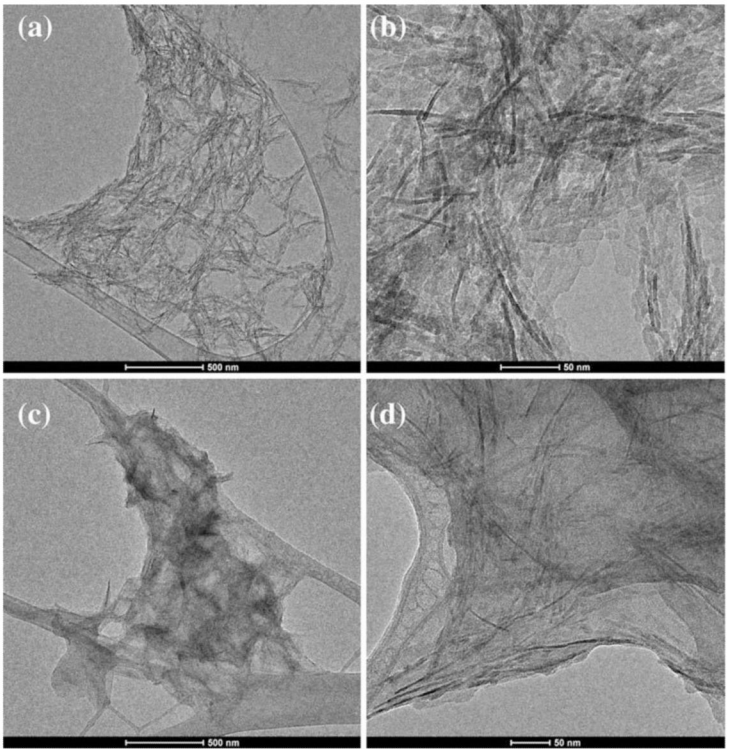

Fig. 2.

a TEM images of HAP nanocrystals that were synthesized using co-precipitation method. **b** Images of high resolution TEM shows that individual fibril-like gelatin aggregate and hydroxyapatite crystals have grown along the fibril direction. **c** Needle-like hydroxyapaptite-gelatin nanocrystals embedded in aminosilica matrix. (GEMOSIL). **d** High resolution TEM image of GEMOSIL. Individual HAP-Gel nanocrystals are visible within the matrix.

NIH-PA Author Manuscript

NIH-PA Author Manuscript

NIH-PA Author Manuscript

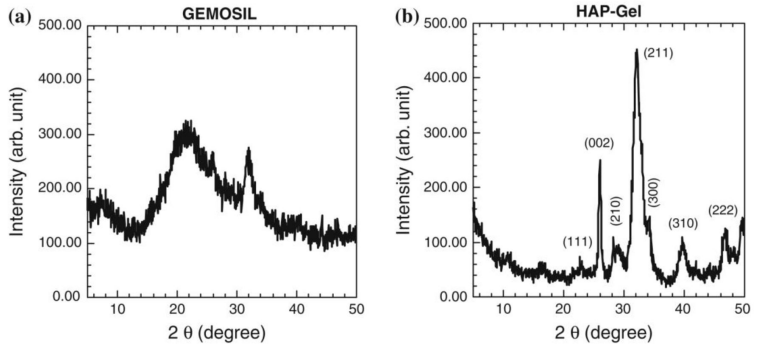

Fig 3.

a X-ray diffraction pattern of GEMOSIL indicates that the crystal structures of hydroxyapatite nanocrystals have been preserved in the aminosilica matrix. The background diffraction pattern that appears as one broad band at 20°represents the typical structure of aminosilica matrix. **b** X-Ray diffraction pattern of a pure HAP-Gel sample. Characteristic peaks of hydroxyapatite are 26°, 32°, 40°, and 47°.

NIH-PA Author Manuscript

NIH-PA Author Manuscript

NIH-PA Author Manuscript

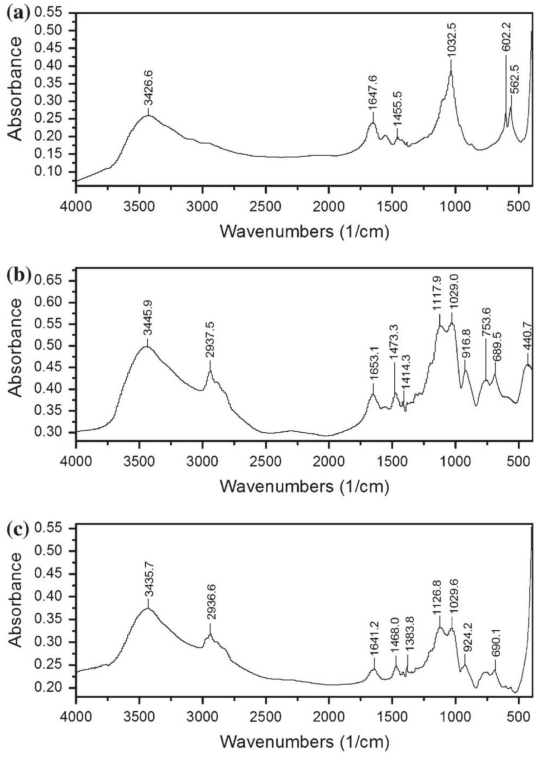

Fig. 4.

a FTIR spectrum of HAP-Gel nanocrytals as prepared from co-precipitation method, **b** FTIR spectrum of a pure enTMOS solid, and **c** FTIR spectrum of GEMOSIL that contains HAP-Gel and aminosilica.

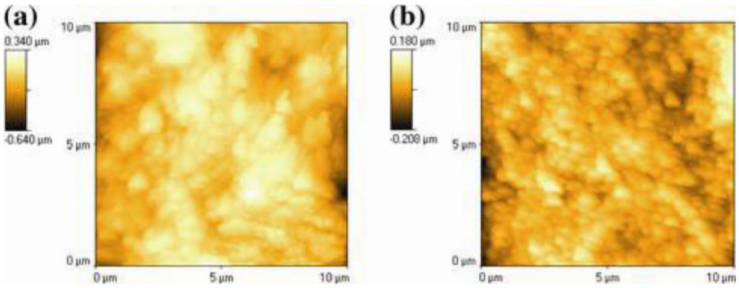

Fig. 5.

a AFM images of the surface of GEMOSIL. The surface spontaneously forms granule-like microstructures. **b** Surface topography of a HAP-Gel film that was synthesized without enTMOS. The surface exhibits higher roughness and more detail features compared to GEMOSIL, indicating the effects of aminosilica as binders and matrix.

NIH-PA Author Manuscript NIH-PA Author Manuscript NIH-PA Author Manuscript

NIH-PA Author Manuscript

NIH-PA Author Manuscript

NIH-PA Author Manuscript

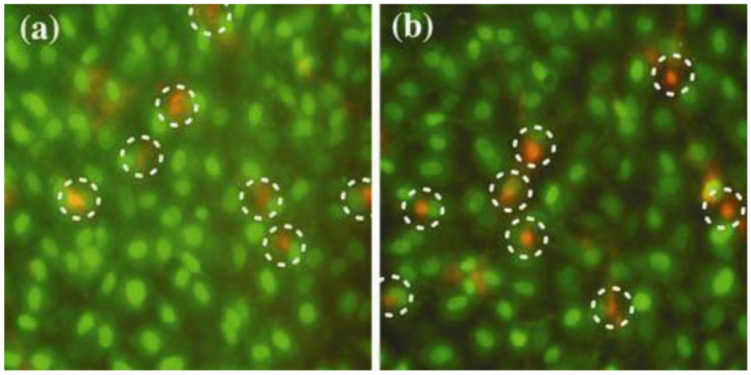

Fig. 6.

Live (green) and death (red, circled by dashed lines) stains for cell viability test. The ratio of the green versus red cells was similar between the **a** GEMOSIL sample and **b** a control dish. (Color figure online).

NIH-PA Author Manuscript

NIH-PA Author Manuscript

NIH-PA Author Manuscript

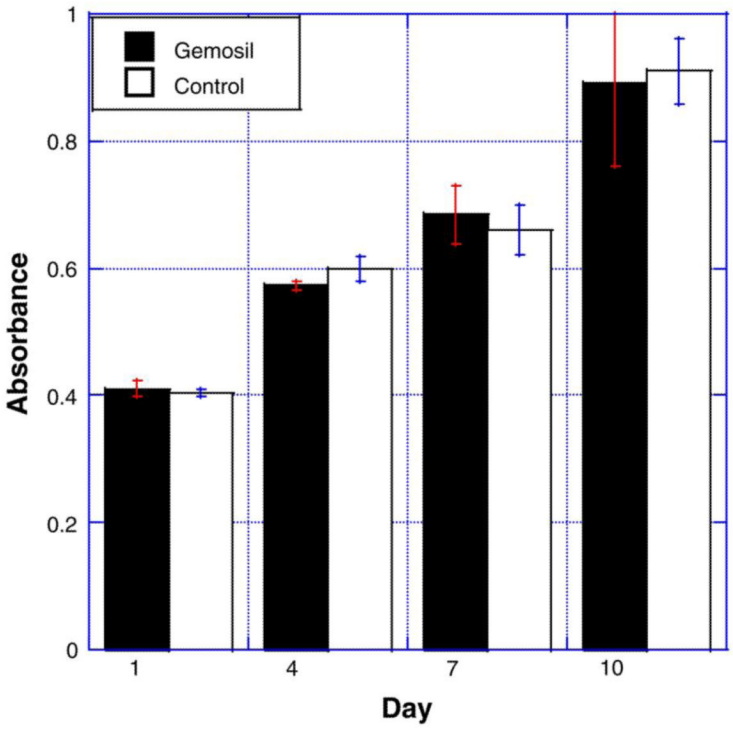

Fig. 7.
Cell growth curves measured by formazan absorbance using CellTiter kits. There are no differences between the GEMOSIL and the control over time.

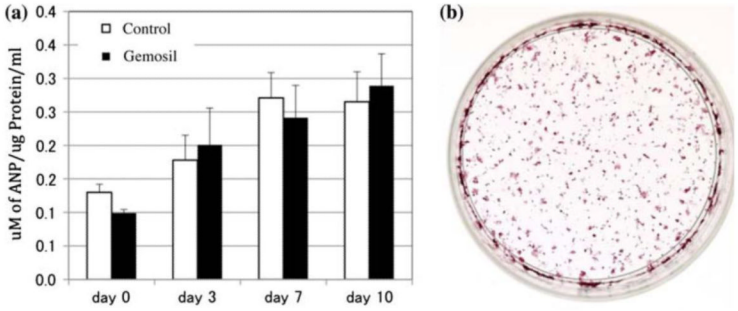

Fig. 8.

a Alkaline phosphatase (ALP) activities of osteoblasts (MC3T3-E1) do not show any differences between the experiment and the control (n = 4). **b** Alizarin red stain for MC3T3-E1 on GEMOSIL (differentiation on day 21) that shows mineral nodules. (Color figure online).

NIH-PA Author Manuscript
NIH-PA Author Manuscript
NIH-PA Author Manuscript